

# Design study of N95 mask sterilization chamber based on UV LED light source

Jiachen Li

(University of Shanghai for Science and Technology, Shanghai 200093, China)

Corresponding Author: Jiachen Li

---

## Abstract

Public health security in all nations is being threatened by the worldwide coronavirus pandemic (COVID-19). Wearing a mask is an effective means of protection since the new coronavirus can spread quickly through respiratory droplets and aerosols in the air. Although the greenhouse gas emissions from their manufacture cannot be understated in the context of global warming, it is vitally necessary to find a solution to the issue of too many masks in order to safeguard the environment. Discarded masks can be environmentally hazardous. As a mild and efficient method of disinfection, UV-C-treated masks can be reused for secondary use, reducing the consumption of masks by the general public to a certain extent. Germicidal UV light can maintain the integrity of KN95 masks, UV light is effective in inactivating the new coronavirus on N95 masks, and UV light is able to disinfect N95 masks. The purpose of this study is to develop a closed disinfection chamber model using UV-LED lamps, which can effectively and uniformly inactivate the new coronavirus on the mask surface, allowing for public reuse of masks and lowering the environmental risks associated with large numbers of contaminated masks.

**Keywords:** Ultraviolet; N95 mask; Germicidal chamber; Lens; Environmental protection

---

Date of Submission: 01-04-2023

Date of acceptance: 12-04-2023

---

## I. INTRODUCTION

Every nation is at great risk from the worldwide COVID-19 pandemic, which is a new coronavirus [1, 2]. Numerous studies indicate that fresh coronaviruses can spread quickly via the air via aerosols and respiratory droplets [3, 4]. Wearing masks is therefore a non-pharmaceutical intervention (NPI) that is inexpensive, simple to execute, and effective [5, 6]. According to several research, wearing a mask lowers the chance of developing new cardiac infections by almost 81% [7].

However, it has been demonstrated that using masks as protection is bad for the environment [8]. The manufacturing and demand for masks have increased significantly since the start of the latest coronary epidemic [9]. Whatever the kind, disposable masks are made of nanofibre plastic, which decomposes into microplastics with a diameter of less than 5 mm by a variety of physical and biological reaction processes when they are abandoned in the open [10]. These microplastic wastes might potentially harm human health [12] because they reach the human diet through fish consumption and persist as contaminants in the environment's soil and water [11]. In the context of global warming, the greenhouse gas emissions from the manufacture of masks should not be understated [13].

Therefore, it is crucial to find environmentally friendly mask disposal methods that meet the demands of their use. The two types of disposable masks that are most commonly used are medical surgical and KN95 masks. KN95 masks are stronger and more effective in terms of protection, making them more deserving of subsequent usage after technical cleaning [15–20]. Governments and the general public in several nations have reportedly started looking into the reuse, disposal, and disinfection of disposable KN95 masks, and the World Health Organization has acknowledged the viability of mask reuse [14].

According to several investigations, UV sterilization preserves the integrity of KN95 masks [22]. Ultraviolet (UV) light has been used often to disinfect surfaces and indoor spaces [27, 28]. The UV-C band, which has a wavelength range of 200 nm to 280 nm, is most efficiently absorbed by nucleic acids and proteins. UVGI functions by destroying the DNA or RNA of germs and viruses to impede reproduction [29]. It is important to note that UVGI is very efficient against viruses, with the bactericidal impact changing with the pathogen's volume [30]. When dealing with fresh coronaviruses, UVGI may also quickly inactivate them; this has been experimentally shown to take only 60 to 70 seconds [30]. However, UV irradiation had no discernible impact on preserving the mask's filtering effectiveness or the overall form of the structure [31]. Low UV doses (10 J/cm<sup>2</sup>) did not significantly alter the mask's filtration capacity, pressure difference, or appearance [21]; high doses (950 J/cm<sup>2</sup>) did not significantly impair the N95 mask's structural integrity and did not result in a filtration efficiency

loss more than 5% [32]. This shows that UV light is efficient at inactivating fresh coronaviruses on N95 masks and that UVC treatment of masks may be utilized for subsequent applications as a mild and effective method of sanitizing masks.

Many of the UV-C devices used now employ ozone-free, small LED light sources, making installation simple in a variety of configurations [21]. However, LED light sources have low irradiance values and wide dispersion angles, which, if uncontrolled, can easily result in a loss of UV radiation. Therefore, the conventional approach is to employ more LED chips, which greatly raises the cost of the materials and results in energy waste, to make up for the low irradiance of LED light sources [30].

The purpose of this study is to create a closed germicidal chamber model using UV LED lamps that can kill new coronaviruses on the surface of masks uniformly and effectively, allowing the general public to reuse masks and to some extent reduce mask consumption. The sustainable usage of N95 masks advocated in this study will aid in lowering the rate of mask disposal, decreasing the chance of environmental contamination, and offering design inspiration and resources for cutting-edge green sustainable development applications.

**1.1.1 Physical model of an LED lens**

According to Lambert's law, the luminous intensity in a given direction,  $I$ , is equal to the luminous intensity in the direction perpendicular to the luminous surface,  $I_0$ , times the cosine of the directional angle, or  $I=I_0\cos$  [36]. The conservation of light range and the conservation of energy are two crucial correlations in optical research [37, 38]. While energy conservation is explained by the fact that, in theory, the luminous flux incident on the lens at an angle is equal to the energy input, light range conservation is explained by the fact that, after a beam of light perpendicular to the wavefront has been reflected and refracted numerous times, the outgoing beam is still perpendicular to the outgoing wavefront and the light range between the incident wavefront and the corresponding point on the outgoing wavefront is constant.

Designing a twin free-form surface, one of which is used to level out the light and the other is used to collimate the light once it has been evened out, will allow you to equally distribute and collimate some of the light output by the LED point source [38]. In Figure 1, the homogenized portion is represented by free-form surface  $A_1$  and the collimated portion is represented by free-form surface  $A_2$ . The typical paraboloid reflecting surface  $A_3$  and the standard sphere-shaped surface  $A_4$  are both preserved by clipping and have their focus point at the origin  $O$ . The planes  $A_5$  and  $A_6$  have no practical optical relevance and are solely utilized to transition from the free-form surface to the paraboloid. With a spherical radius of  $R$  and an infinite plane, surface  $L$  and plane  $L'$  are introduced to virtual spherical receiving surfaces and virtual planar receiving surfaces, respectively.

Figure 1 shows the origin of the LED point source  $O$ .  $\varphi_M$  is the angle of separation between the refracted and reflected portions, which is also the greatest angle of incidence of the refracted part.  $\varphi_m$  is the angle of incidence of the refracted part. incidence angle larger than the  $M$  portion of the light via the parabolic reflection collimated out; incident angle less than  $\varphi_M$  part of the light through the double free surface twice refraction. The free-form surfaces  $A_1$  and  $A_2$  receive the light incident along the  $Y$ -axis at light distances of  $h$  and  $d$ , respectively, where  $d$  is also the lens's thickness and both values are arbitrary. In relation to the refraction part, the point  $P_m$  is where light enters the lens, the point  $Q_m$  is where it leaves the lens, and the point  $L_m$  on the virtual plane is where the light finally falls at the parting angle.

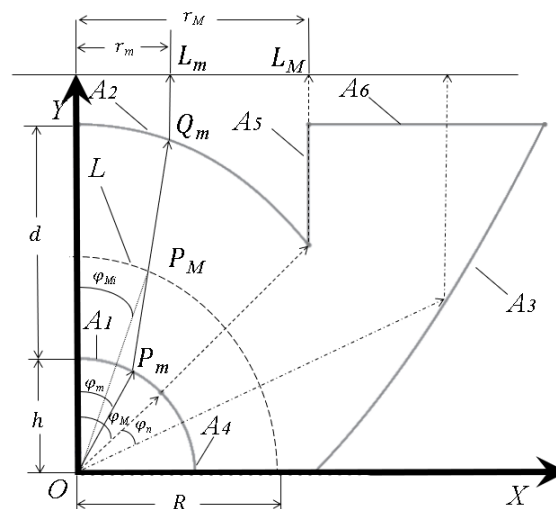


**Figure1: Schematic diagram of the solution section of a hyperbolic uniform collimated lens**

When the radius of the virtual sphere R takes a larger value, the angle between the line connecting point O and P<sub>m</sub> and the Y axis is roughly equal to the i-th partition angle of M, denoted as M<sub>i</sub>, in the XY plane shown in Figure 1. The partition angle M is equally divided into n equal parts, and the intersection point of the first refraction and the virtual sphere is located at P<sub>M</sub>. The angle connection equation of the uniform light component before and after the first light refraction, established using the virtual spherical receiving surface previously mentioned, according to the conservation of optical energy relationship, produces [37]:

$$\varphi_m = \arcsin \sqrt{\frac{\cos\varphi_{Mi} - 1}{\cos\varphi_M - 1}} \quad (1)$$

Suppose the coordinates of the point P<sub>m</sub> are (x<sub>i</sub>, y<sub>i</sub>), then the coordinates of the point P<sub>M</sub> are (Rsinφ<sub>Mi</sub>, Rcosφ<sub>Mi</sub>).

The unit vector of the incident light line OP<sub>m</sub> is:

$$m_i = \left( \frac{x_i}{\sqrt{x_i^2 + y_i^2}}, \frac{y_i}{\sqrt{x_i^2 + y_i^2}} \right) \quad (2)$$

The unit vector of the outgoing ray P<sub>m</sub>P<sub>M</sub> is:

$$M_i = \left( \frac{R\sin\varphi_{Mi} - x_i}{\sqrt{(R\sin\varphi_{Mi} - x_i)^2 + (R\cos\varphi_{Mi} - y_i)^2}}, \frac{R\cos\varphi_{Mi} - y_i}{\sqrt{(R\sin\varphi_{Mi} - x_i)^2 + (R\cos\varphi_{Mi} - y_i)^2}} \right) \quad (3)$$

The normal vector at the point P<sub>m</sub> can be found according to Snell's law as follows:

$$N_i(N_{i-x}, N_{i-y}) = nm_i - M_i \quad (4)$$

$$y - y_i = \left( -\frac{N_{i-y}}{N_{i-x}} \right)^{-1} \cdot (x - x_i) \quad (5)$$

The i+1st incident ray's linear equation, which corresponds to m, can be easily found from the geometric relationship in the diagram. The linear equation is then combined with equation (5), and the resulting intersection point can be roughly identified as the i+1st coordinate point on the free surface A<sub>1</sub>.

Assume that the light OP<sub>m</sub> has an optical range of and that the second refraction takes place at point Q<sub>m</sub> on the free-form surface A<sub>2</sub> with coordinates (r<sub>m</sub>, y<sub>i</sub>') for the collimated portion of the light. The relationship based on the conservation of optical energy results in the following when using the virtual planar receiving surface to determine the angular connection between the collimated part of the light before and after the second refraction:

$$r_m = \frac{r_M \sin\varphi_m}{\sin\varphi_M} \quad (6)$$

The conservation of light range relationship gives [38]:

$$y_i' = \frac{\{-[(1-a)d - a\rho]a - \rho\cos\varphi_m\} - \sqrt{\{[(1-a)d - a\rho]a + \rho\cos\varphi_m\}^2 - (a^2 - 1)C}}{a^2 - 1} \quad (7)$$

In formula  $a = \frac{n_1}{n_2}$ ,  $C = [(1-a)d - a\rho]^2 - (r_m - \rho\sin\varphi_m)^2 - (\rho\cos\varphi_m)^2$ , n<sub>1</sub> is the refractive index of air and n<sub>2</sub> is the refractive index of the lens.

Using the intersection of the light incident along the y-axis with the free-form A<sub>1</sub> as the beginning point, equation (5) may be used to solve for the set of points in the first quadrant of the free-form A<sub>1</sub> profile after n repetitions. The set of points on the free-form surface A<sub>2</sub> may be used to solve for the set of points on the free-form surface A<sub>1</sub> from equations (6) and (7). A polynomial curve may be fitted to the curve to provide the equation.

In this investigation, the lens contour line was chosen to have a lens thickness of d=15mm, a virtual spherical radius of R=1000mm, and a maximum spot radius of r<sub>M</sub>=10mm. The starting condition was the splitting angle M=45°, and the point sets of the free-form surfaces A<sub>1</sub> and A<sub>2</sub> were fitted to polynomial curves. The beginning point of solution's coordinates (0, 5) were established, i.e., h=5mm.

The polynomial equation for the fitted curve was entered into the SolidWorks modelling program, and a standard parabola with a focal length of 5 mm was produced with the corresponding connecting line. This parabola was then cut and rotated 360 degrees around the Y-axis to create a solid model of the lens with an overall thickness D of 15 mm, an emitting surface radius R<sub>1</sub> of 20 mm, and an incident surface radius R<sub>2</sub> of 10 mm.

**1.1.2 Simplified model of a mouthpiece**

As shown in the mask state and simplified model diagram in Figure 2.1 (a), the folded KN95 half-mask specified in GB2626-2019 "Respiratory protection - Self-absorbing filtered anti-particulate respirator" was chosen as the study's object. Its dimensions are 160 mm in length by 120 mm in width[39].

The N95 mask's thickness is negligible when it is folded, so to make it easier to analyse the total germicidal dose applied to the mask surface, the mask's overall shape can be simplified to resemble a receiving plane, as shown in Figure 2.1 (c), with dimensions  $L'$  (length)  $D'$  (width) of 160 mm 120 mm. The mask's unfolded state is The length of the mask is lowered when it is unfurled, with the amount of reduction varied depending on the individual use, such that it is less than 160mm in Figure 2.1 (b); for width, the mask attaching hook in the sterilisation chamber restricts it to 120mm. For convenience of analysis, the unfolded mask is reduced to a three-dimensional model with dimensions of  $l'$  (length) x  $d'$  (width) of 160 mm x 120 mm, which is made up of the planar model in Figure 2.1(c), as in Figure 2.1 (d). There is no spatial reflection or influence on UV dosage due to space reflection because the inside surface of the germicidal chamber is black and has a zero reflectivity.

**1.1.3 Closed germicidal chamber model**

The design model of the left and right symmetric closed germicidal chamber shown in Figure 2, the mask bend overlap part will reduce the effect of UV irradiation, so the mask to maintain the unfolded state using the hanging arrangement in the chamber. LED light source and lens combination lamps arranged in the mask directly below. The specific values of distances  $M$  and  $N$  in the figure are presented in the optical model in Section 2. The LED light source and lens combination lamps and lanterns are arranged underneath the mask. The specific values of the distances  $M$  and  $N$  are presented in the optical model in Section 2.

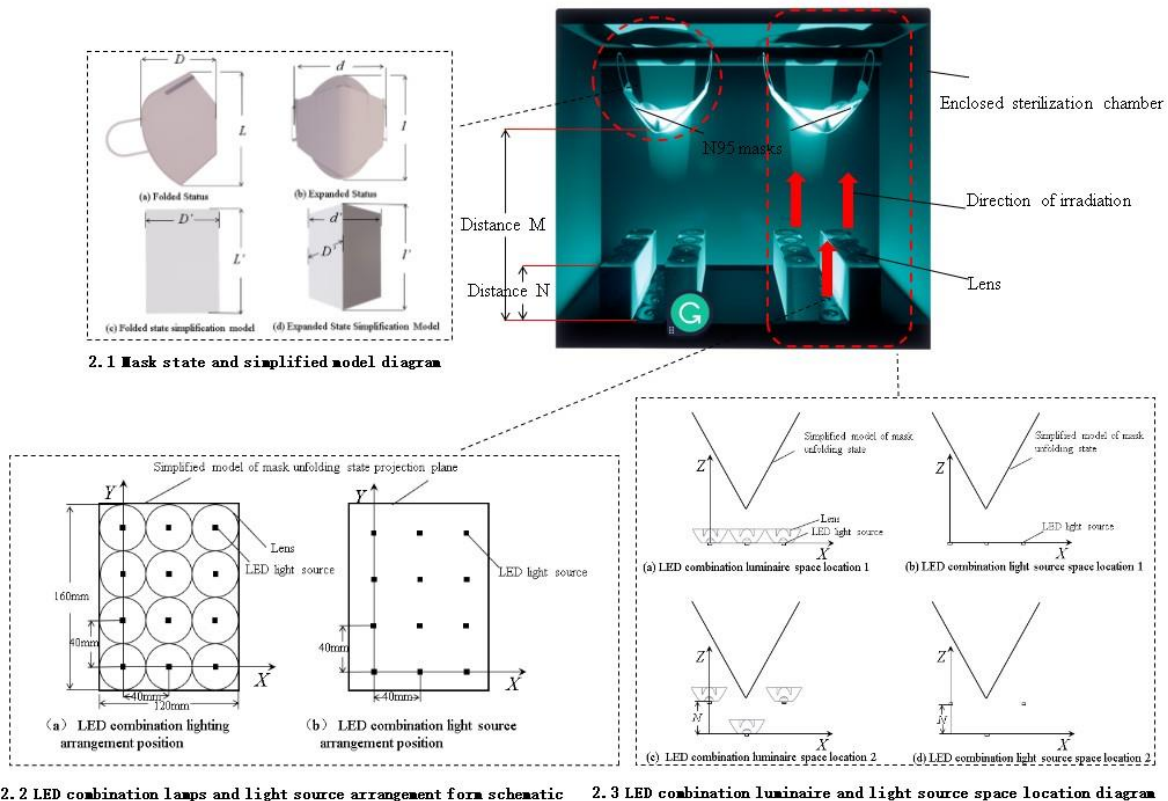
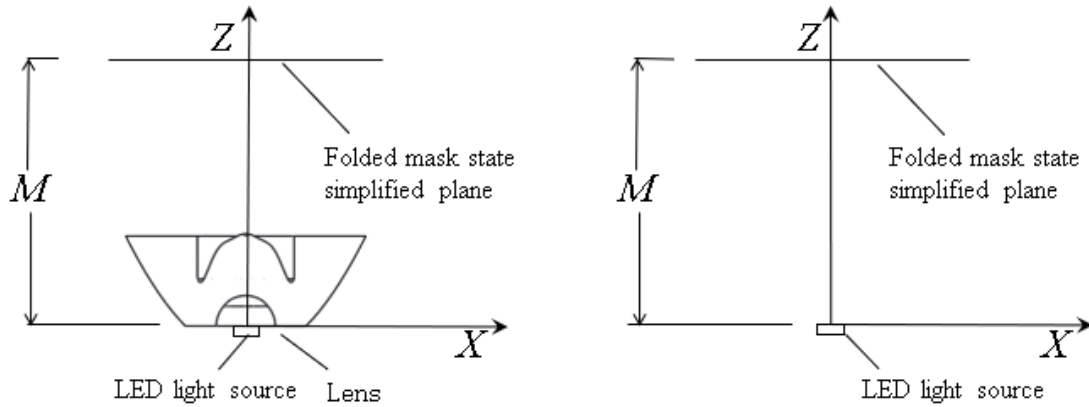


**Figure2: Internal structure of the closed germicidal chamber model with combined LED luminaires and light source arrangement**

**1.2 Optical models**

**1.2.1 Single LED luminaire with light source arrangement form**

For the simplified model in Fig. 2.1(c), an optical model as shown in Fig. 3 is created in TracePro. The analysis compares the average irradiance, irradiation spot radius, and received beam half-angle of a single LED light source in the plane of the simplified model of the mouthpiece located at different distances  $M$  with and without a lens.



(a) LED luminaire arrangement position

(b) LED light source arrangement position

Figure3: Diagram of a single LED luminaire with light source arrangement

**1.2.2 Combination of LED luminaires and light source arrangement forms**

The distribution of the combined forms of multiple lenses in the XY plane was produced as indicated in Figure 2.2 in order to obtain the most complete distribution of the combined beams of multiple lenses on the projection of the model surface in Figure 2.1(d).

The three-dimensional surface of the cabin mask is depicted in Figure 2.1(d) with various distances from the luminaire at various points: the cabin mask is closest to the lens exit surface at the fold line and farthest away at the mask ear strap connection. This implies that the unfolded masks have different spatial heights, and that the difference in distance over the same UV action period is a significant factor in the ineffective and uneven sterilisation. As a result, the configuration in the XZ plane takes on the appearance in Figure 2.3.

A physical model of the corresponding spatial position is established in TracePro, as shown in Table 1, to compare and study the average irradiance, irradiance uniformity, and the effective irradiance range of the mask surface at the same distance M, at different distances N. Here, the distance N denotes the distance of the luminaire away from the plane where the X axis is located. The overall minimum effective germicidal time, the ideal number of cycles, and the overall germicidal uniformity are evaluated based on the results of the light tracing and when combined with the necessary irradiance dose range on the mask surface.

**Table 1 Comparative analysis of LED combination luminaires and light sources**

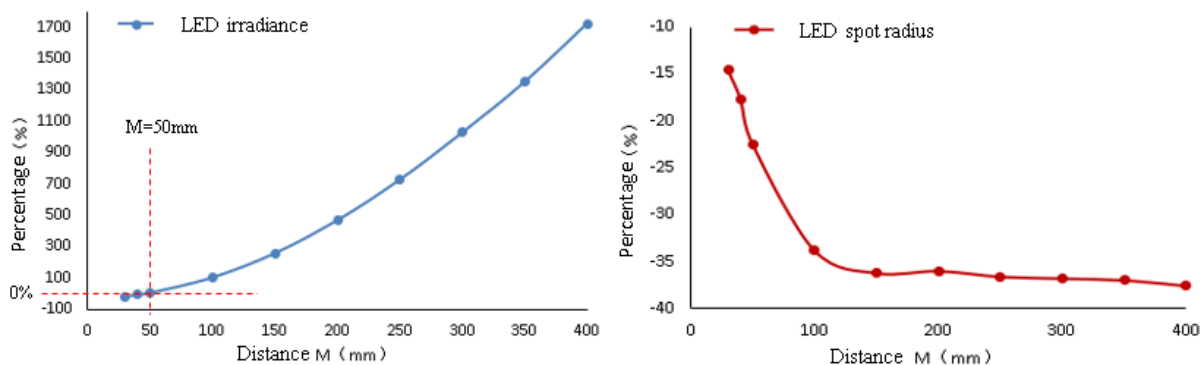
No.	Control group	Simulation group	Control group form	Simulation group format
1	N=0	N=15mm	LED Luminaire	LED Luminaire
2	N=0	N=30mm	LED Luminaire	LED Luminaire
3	N=0	N=45mm	LED Luminaire	LED Luminaire
4	N=0	N=15mm	LED Light source	LED Luminaire
5	N=0	N=30mm	LED Light source	LED Luminaire
6	N=0	N=45mm	LED Light source	LED Luminaire

Using the 3D modelling programme SolidWorks, the aforementioned models were created. Next, optical simulation software TracePro was used to create optical models of individual LED luminaires and LED sources, as well as various combinations, as shown in the table above, against which light tracing simulations were performed.

**II. RESULT AND DISCUSSION**

**1.1 Individual LED luminaires with light sources**

In terms of the LED luminaire in relation to the LED light source, the irradiance values are reported as a percentage increase or reduction. Figure 4 displays the relationship between the average irradiance received in the plane of the simplified model of the masks placed at various distances M and the radius of the irradiated spot.



(a) Average irradiance simulation results (b) Spot radius simulation results  
**Figure4: Single LED luminaire with lamp source simulation results**

The average irradiance received by the plane is divided by the distance  $M$ , which is equal to 50mm, in Figure 4(a), and when the distance is greater than 50mm, at the same distance  $M$ , the percentages shown are positive. It can be seen from the percentage size that the average irradiance of the LED luminaire is significantly higher than the average irradiance of the LED light source. This trend exhibits an exponential tendency with quick multiplicative growth as  $M$  rises.

As shown in Figure 4(b), when comparing the spot radius created by an LED light source and an LED luminaire in a plane, the spot radius created by the LED light source must continue to grow as the distance grows, whereas the spot radius created by the LED luminaire changes less over time. This creates a trend in the figure of increasing absolute values of the percentage. From the spot radius with distance change law, it can be observed that without a lens, LED light sources consistently disperse light as the distance increases. The performance of LED light sources is greatly enhanced by lens collimation uniform light.

### 1.2 Combined LED luminaires and light sources

According to the various distances  $N$  provided in Table 1 and in the full cloth form of Figures 2.2 and 2.3, respectively, the light tracing was performed for the integrated LED luminaires and the light source analysis model. The combined LED luminaires' irradiance results are expressed in Figure 5 as a percentage increase or reduction of the LED luminaires relative to the LED light source. The rise in average luminaire irradiance between the combined LED luminaires at different distances  $N$  is more pronounced the larger the value of  $N$ ; the difference is more pronounced up to  $N=50$ mm, after which there is a constant trend.

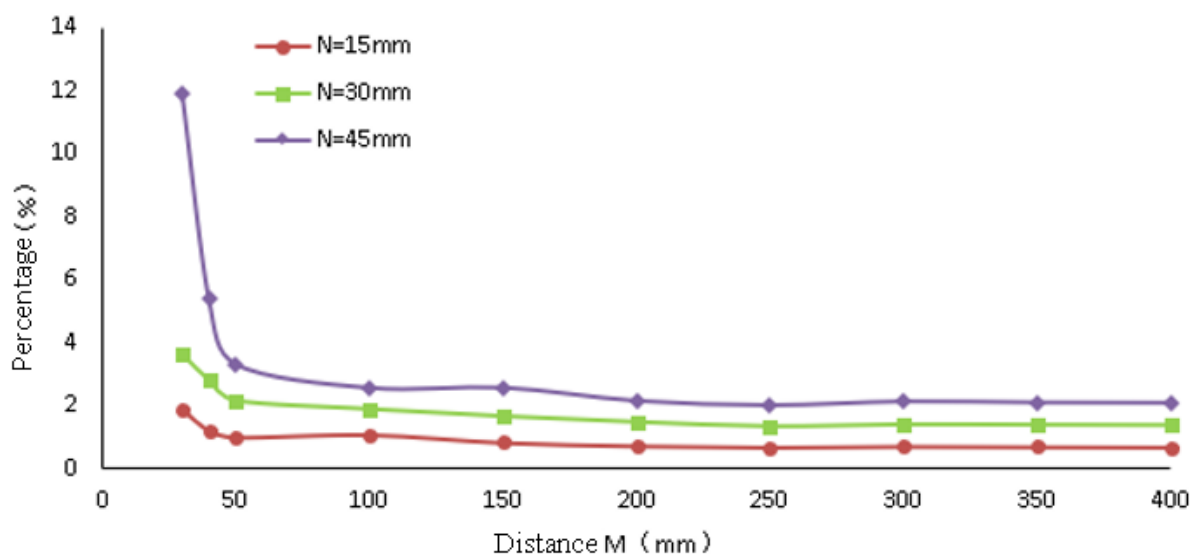


**Figure5: Average irradiance of combined LED luminaires**

Figure 6 compares the findings for the combined LED luminaires' irradiance uniformity. Despite the luminaires' staggered arrangement in the XZ plane, at a distance  $M$  of 180 mm, the uniformity is nearly similar, and at this distance, the layout virtually has no impact on the irradiation's uniformity on the mask surface. The luminaire configuration with  $N=0$  mm creates the least uniformity at a distance  $M$  more than 210 mm and the

highest uniformity at a distance M less than 180 mm. The graph also shows that, after M=210mm, the difference in uniformity between the various distance values N stays steady.

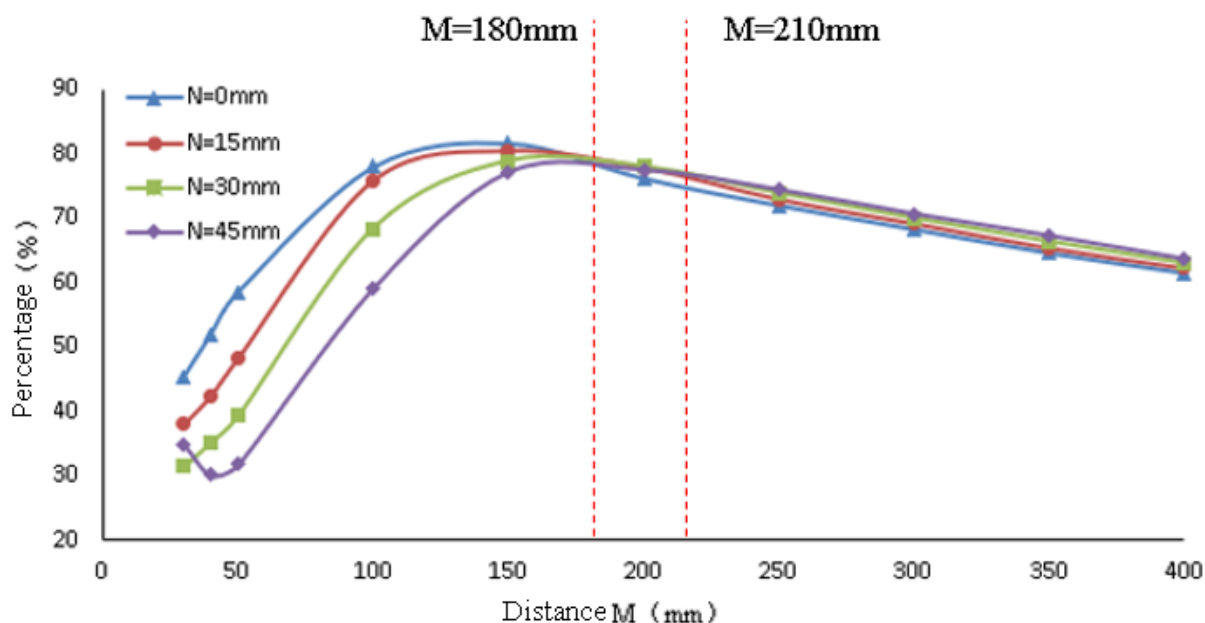


Figure6: Irradiance uniformity of combined LED luminaires

### III. CONCLUSION

In a closed germicidal chamber model, this study qualitatively discusses the average irradiance and irradiance uniformity of the mask surface for various combinations of UVC LED lamps and LED light sources, and then looks into the variation of these two crucial factors that influence germicidal effectiveness.

The study presented above leads to the following conclusions: 1) LED luminaires made of lenses and LED light sources have a substantial impact on the aggregation of stray LED light sources by reducing the spot radius and increasing average irradiance to a certain amount; 2) When placed in the same configuration, LED luminaires may greatly increase irradiance, and after a certain distance, the distance between the receiving surface and the light source has little to no impact on the amount of irradiance; 3) When comparing various configurations of numerous LED luminaires, staggered configurations have a little advantage in increasing average irradiance, and the effect on uniformity is about the same at a certain distance. The distance between the receiving surface and the light source has little bearing on irradiance; 3) when using multiple LED luminaires in different configurations, the staggered arrangement improves average irradiance while maintaining nearly the same uniformity over a certain distance.

This study explores new approaches to reducing the environmental damage brought on by excessive mask disposal. It also offers an environmentally friendly response to the quest for effective germicidal applications and creative uses of UV germicidal LED light sources.

### REFERENCES

- [1]. Tian D, Sun Y, Zhou J, et al. The global epidemic of the SARS-CoV-2 delta variant, key spike mutations and immune escape[J]. *Frontiers in immunology*, 2021, 12.
- [2]. Zhou X, Ye Q. Cellular immune response to COVID-19 and potential immune modulators[J]. *Frontiers in Immunology*, 2021, 12: 646333.
- [3]. Tang S, Mao Y, Jones R M, et al. Aerosol transmission of SARS-CoV-2? Evidence, prevention and control[J]. *Environment international*, 2020, 144: 106039.
- [4]. Zuo YY, Uspal WE, Wei T. Airborne transmission of COVID-19: aerosol dispersion, lung deposition, and virus-receptor interactions. *ACS Nano*. 2020;14:16502–24.
- [5]. Li Y, Liang M, Gao L, et al. Face masks to prevent transmission of COVID-19: A systematic review and meta-analysis[J]. *American Journal of Infection Control*, 2021, 49(7): 900-906.
- [6]. Chowdhury H, Chowdhury T, Sait S M. Estimating marine plastic pollution from COVID-19 face masks in coastal regions[J]. *Marine Pollution Bulletin*, 2021, 168: 112419.
- [7]. Mghili B, Analla M, Aksissou M. Face masks related to COVID-19 in the beaches of the Moroccan Mediterranean: an emerging source of plastic pollution[J]. *Marine Pollution Bulletin*, 2022, 174: 113181.
- [8]. Du H, Huang S, Wang J. Environmental risks of polymer materials from disposable face masks linked to the COVID-19 pandemic[J]. *Science of The Total Environment*, 2022: 152980.
- [9]. Li B, Huang Y, Guo D, et al. Environmental risks of disposable face masks during the pandemic of COVID-19: Challenges and management[J]. *Science of the Total Environment*, 2022, 825: 153880.

- [10]. Barbanera M, Marconi M, Peruzzi A, et al. Environmental assessment and eco-design of a surgical face mask[J]. *Procedia CIRP*, 2022, 105: 61-66.
- [11]. Aragaw T A. Surgical face masks as a potential source for microplastic pollution in the COVID-19 scenario[J]. *Marine Pollution Bulletin*, 2020, 159: 111517.
- [12]. Selvaranjan K, Navaratnam S, Rajeev P, et al. Environmental challenges induced by extensive use of face masks during COVID-19: A review and potential solutions[J]. *Environmental Challenges*, 2021, 3: 100039.
- [13]. Ray S S, Lee H K, Huyen D T T, et al. Microplastics waste in environment: A perspective on recycling issues from PPE kits and face masks during the COVID-19 pandemic[J]. *Environmental Technology & Innovation*, 2022: 102290.
- [14]. World Health Organization (WHO). Rational use of personal protective equipment for coronavirus disease 2019 (COVID-19), vol.2019. WHO; 2020. p. 1e7
- [15]. Johnson D F, Druce J D, Birch C, et al. A quantitative assessment of the efficacy of surgical and N95 masks to filter influenza virus in patients with acute influenza infection[J]. *Clinical Infectious Diseases*, 2009, 49(2): 275-277.
- [16]. Verma S, Dhanak M, Frankenfield J. Visualizing the effectiveness of face masks in obstructing respiratory jets[J]. *Physics of Fluids*, 2020, 32(6): 061708.
- [17]. Rengasamy S, Eimer B C, Szalajda J. A quantitative assessment of the total inward leakage of NaCl aerosol representing submicron-size bioaerosol through N95 filtering facepiece respirators and surgical masks[J]. *Journal of occupational and environmental hygiene*, 2014, 11(6): 388-396.
- [18]. Balazy A, Toivola M, Adhikari A, et al. Do N95 respirators provide 95% protection level against airborne viruses, and how adequate are surgical masks?[J]. *American journal of infection control*, 2006, 34(2): 51-57.
- [19]. He X, Reponen T, McKay R T, et al. Effect of particle size on the performance of an N95 filtering facepiece respirator and a surgical mask at various breathing conditions[J]. *Aerosol Science and Technology*, 2013, 47(11): 1180-1187.
- [20]. Eshbaugh J P, Gardner P D, Richardson A W, et al. N95 and P100 respirator filter efficiency under high constant and cyclic flow[J]. *Journal of occupational and environmental hygiene*, 2008, 6(1): 52-61.
- [21]. Ju J T J, Boisvert L N, Zuo Y Y. Face masks against COVID-19: Standards, efficacy, testing and decontamination methods[J]. *Advances in Colloid and Interface Science*, 2021, 292: 102435.
- [22]. Sarkis-Onofre R, do Carmo Borges R, Demarco G, et al. Decontamination of N95 respirators against SARS-CoV-2: A scoping review[J]. *Journal of dentistry*, 2021, 104: 103534.
- [23]. Chua M H, Cheng W, Goh S S, et al. Face masks in the new COVID-19 normal: materials, testing, and perspectives[J]. *Research*, 2020, 2020.
- [24]. Tcharkhtchi A, Abbasnezhad N, Seydani M Z, et al. An overview of filtration efficiency through the masks: Mechanisms of the aerosols penetration[J]. *Bioactive materials*, 2021, 6(1): 106-122.
- [25]. Ou Q, Pei C, Kim S C, et al. Evaluation of decontamination methods for commercial and alternative respirator and mask materials—view from filtration aspect[J]. *Journal of Aerosol Science*, 2020, 150: 105609.
- [26]. Bošković I, Gallo C, Wallace M B, et al. COVID-19 pandemic and personal protective equipment shortage: protective efficacy comparing masks and scientific methods for respirator reuse[J]. *Gastrointestinal endoscopy*, 2020, 92(3): 519-523.
- [27]. Su C, Lau J, Gibbs S G. Student absenteeism and the comparisons of two sampling procedures for culturable bioaerosol measurement in classrooms with and without upper room ultraviolet germicidal irradiation devices[J]. *Indoor and Built Environment*, 2016, 25(3): 551-562.
- [28]. Su C, Lau J, Yu F. A case study of upper-room UVGI in densely-occupied elementary classrooms by real-time fluorescent bioaerosol measurements[J]. *International journal of environmental research and public health*, 2017, 14(1): 51.
- [29]. Gilbert R M, Donzanti M J, Minahan D J, et al. Mask reuse in the COVID-19 pandemic: creating an inexpensive and scalable ultraviolet system for filtering facepiece respirator decontamination[J]. *Global Health: Science and Practice*, 2020, 8(3): 582-595.
- [30]. Torres A E, Lyons A B, Narla S, et al. Ultraviolet-C and other methods of decontamination of filtering facepiece N-95 respirators during the COVID-19 pandemic[J]. *Photochemical & Photobiological Sciences*, 2020, 19(6): 746-751.
- [31]. Gnatta J R, de Souza R Q, de Santana Lemos C, et al. Safety in the practice of decontaminating filtering facepiece respirators: A systematic review[J]. *American journal of infection control*, 2021, 49(6): 825-835.
- [32]. Lindsley W G, Martin Jr S B, Thewlis R E, et al. Effects of ultraviolet germicidal irradiation (UVGI) on N95 respirator filtration performance and structural integrity[J]. *Journal of occupational and environmental hygiene*, 2015, 12(8): 509-517.
- [33]. Ruiz-Bastián M, Rodríguez-Tejedor M, Rivera-Núñez M A, et al. Detection of SARS-CoV-2 genomic RNA on surgical masks worn by patients: Proof of concept[J]. *Enfermedades infecciosas y microbiología clínica (English ed.)*, 2021, 39(10): 528.
- [34]. van der Vossen J M B M, Fawzy A, Ouwens A M T, et al. Effective ultraviolet C light disinfection of respirators demonstrated in challenges with *Geobacillus stearothermophilus* spores and SARS-CoV-2 virus[J]. *Journal of Hospital Infection*, 2022, 122: 168-172.
- [35]. Dunn E F, Akhtar A, Dunn A, et al. Evaluating an Ultraviolet C System for Use During SARS-CoV2 Pandemic and Personal Protective Equipment Shortage[J]. *Advances in radiation oncology*, 2021, 6(2): 100636.
- [36]. Dong Wenjuan. LED secondary light distribution lens design [D]. Jiangsu University, 2017.
- [37]. Fu Qian, Su Chengyue, Xue Tao, et al. A virtual target surface-based design method for LED uniform light intensity lenses[J]. *Photovoltaic Engineering*, 2013, 40(11): 46-50.
- [38]. Meng Xiangxiang, Liu Weiqi, Feng Rui, et al. Design of collimated lenses for double free-form LED uniform illumination[J]. *Journal of Photonics*, 2014 (8): 10-15.
- [39]. Respiratory Protection - Self-priming Filtered Particulate Respirators (GB 2626-2019)
- [40]. Golladay G J, Leslie K A, Zuelzer W A, et al. Rationale and process for N95 respirator sanitation and reuse in the coronavirus disease 2019 (COVID-19) pandemic[J]. *Infection Control & Hospital Epidemiology*, 2022, 43(1): 40-44.
- [41]. Hummel A, Ergai A, Spiva L A, et al. Rapid design and implementation of a UVC decontamination room[J]. *Scientific Reports*, 2022, 12(1): 1-7.